

Theory of light-induced drift of a one-component gas in a capillary

V. G. Chernyak and E. A. Subbotin

A. M. Gor'kiĭ Ural State University

(Submitted 15 February 1995)

Zh. Éksp. Teor. Fiz. **108**, 227—239 (July 1995)

The surface and collisional mechanisms of light-induced drift of a one-component gas in a capillary are investigated theoretically. These mechanisms are based on various interactions of the excited and unexcited particles with the surface of the capillary and with one another. The kinetic equations for the velocity distribution functions of the excited and unexcited particles are solved numerically by the discrete-ordinate method. The velocity profiles and the gas fluxes, averaged over the transverse cross section of the capillary, are calculated as a function of the Knudsen number and the ratio of the radiative decay rate to the intermolecular collision rate. © 1995 American Institute of Physics.

1. INTRODUCTION

A theory of light-induced free-molecular surface drift of a one-component gas in a capillary is presented in Refs. 1 and 2. It is shown that the Bennett peak and dip in the velocity distributions of these particles are deformed differently for various interactions of the excited and unexcited particles with the surface of the capillary, and they do not cancel one another. The asymmetry of the total distribution function relative to the zero value of the projection of the molecular velocity on the direction of propagation of the light wave determines the motion of the absorbing gas as a whole. We note that the possibility, in principle, of surface light-induced drift was first predicted in Ref. 3. In Ref. 4 calculations of this phenomenon were carried out in the hydrodynamic approximation. The main deficiency of the results obtained in Ref. 4 are that the light-induced slip boundary condition for the Navier–Stokes equation was derived under the assumption that the particle-velocity distribution function remains unchanged across the Knudsen layer.

In Refs. 5–8, collisional light-induced drift in a channel formed by two infinite parallel plates was calculated. This phenomenon owes its existence to the difference in interaction cross sections of the excited and unexcited particles. In Refs. 6–8, surface light-induced drift was also studied taking into account the spatial nonuniformity of the distribution function. In Ref. 6 this was done for both small and large values of the Knudsen number (Kn), in Ref. 7 for arbitrary values of Kn, and in Ref. 8 for small values of Kn ($\text{Kn} \leq 0.2$).

A kinetic theory of the surface and collisional mechanisms of light-induced drift of a one-component gas in a cylindrical capillary was developed in Ref. 9 for arbitrary Kn. However, the results obtained there are limited by the assumption that the radiative decay rate Γ_m of an excited level is small compared to the intermolecular collision rate γ_n , i.e., $\Gamma_{mn} = \Gamma_m / \gamma_n \ll 1$. Moreover, the Bubnov–Galerkin method used in Ref. 9 to solve the integral–moment equations for the partial velocities and viscous stresses did not make it possible to investigate the light-induced drift velocity profile and its evolution as the flow regime changed from hydrodynamic to free-molecular.

Our objective in the present work is to develop a kinetic theory of the surface and collisional mechanisms of light-induced drift of a one-component gas in a capillary for arbitrary values of Kn and the frequency parameter Γ_{mn} , and to calculate the velocity profile and the mean gas flux over the cross section of the capillary. This multiparameter, mathematically complicated problem can probably only be solved numerically. The optimal method appears to be the method of discrete ordinates, which is based on replacing the continuous six-dimensional phase space by a discrete space. Numerical results obtained with guaranteed accuracy are also of particular interest in that they can be used to test various approximate theories of light-induced drift.

2. ASSUMPTIONS AND BASIC EQUATIONS

We study the steady motion of a one-component gas in a circular capillary under the action of resonant optical radiation propagating along the z axis of the capillary. Let the length L of the capillary be much greater than its radius R_0 , so that distortions of the velocity field at the ends of the capillary can be neglected. The radiation is absorbed by the gas particles in electronic or vibrational–rotational transitions from the ground state n to an excited state m . The frequency ω of the monochromatic radiation is offset from the center ω_{mn} of the absorption line by $\Omega = (\omega - \omega_{mn}) \ll \omega, \omega_{mn}$. As a result of the Doppler effect, only particles with velocities \mathbf{v} such that $\mathbf{k}\mathbf{v} = \Omega$, where \mathbf{k} is the wave vector, interact most efficiently with the radiation. Particles that have absorbed radiation have a different collision cross section. Thus, the absorbing gas can be regarded as a binary gaseous mixture in which the particles have the same masses but different interaction cross sections. Particle exchange between components of the mixture is possible as a result of radiative decay of an excited level, as well as collisional and stimulated transitions.

The velocity distributions f_m and f_n of the excited and unexcited particles, respectively, have a peak and a Bennett dip,¹⁰ respectively, near the resonance values $v_z = \Omega/k$, where v_z is the projection of the velocity vector \mathbf{v} on the z axis. For $\Omega \neq 0$, these distributions are asymmetric with respect to $v_z = 0$. Consequently, oppositely directed macro-

scopic fluxes \mathbf{J}_m and \mathbf{J}_n of excited and unexcited particles, respectively, exist along the capillary. If the probabilities that excited and unexcited particles pass through the capillaries are different because the interactions of the two types of particles with the surface and the transport cross sections are different, then there exists a resulting flux $\mathbf{J} = \mathbf{J}_m + \mathbf{J}_n$ —the light-induced drift.

In the two-level approximation, the distribution functions f_m and f_n satisfy the following system of kinetic equations¹⁰:

$$\mathbf{v}\nabla f_m = \frac{1}{2} \kappa(\mathbf{v})\Gamma_m(f_n - f_m) - \Gamma_m f_m + S_m, \quad (1)$$

$$\mathbf{v}\nabla f_n = -\frac{1}{2} \kappa(\mathbf{v})\Gamma_m(f_n - f_m) + \Gamma_m f_m + S_n,$$

where

$$\kappa(\mathbf{v}) = \frac{4|g_{mn}|^2\Gamma}{\Gamma_m[\Gamma^2 + (\Omega - \mathbf{k}\mathbf{v})^2]}, \quad g_{mn} = \frac{E_0 d_{mn}}{2\hbar},$$

Γ_m is the radiative decay constant, Γ is the homogeneous half-width of the absorption line, S_m and S_n are the Boltzmann collision integrals, E_0 is the amplitude of the electric field, d_{mn} is the transition dipole moment for the transition $m-n$, \hbar is Planck's constant, and $\kappa(\mathbf{v})$ is the saturation parameter characterizing the probability of stimulated transitions and is proportional to the radiative intensity I .

Let the gas and the capillary have the same coordinate-independent temperature T . We also assume that collisions of molecules with the capillary surface are elastic. Then Maxwell's specular diffusion model can be chosen to give the boundary conditions for Eqs. (1). According to this model, a fraction ε_j of the particles in state j after a collision with the surface spreads out diffusively with Maxwell's velocity distribution f_j^s , while the fraction $1 - \varepsilon_j$ is reflected specularly, i.e.,

$$f_j^+(\mathbf{v}) = \varepsilon_j f_j^s(\mathbf{v}) + (1 - \varepsilon_j) f_j^-(\mathbf{v} - 2(\mathbf{v}\mathbf{n})\mathbf{n}), \quad \mathbf{v}\mathbf{n} > 0, \quad (2)$$

$$f_j^s = n_j^s \left(\frac{m_0}{2\pi k_B T} \right)^{3/2} \exp\left(-\frac{m_0 v^2}{2k_B T}\right), \quad j = m, n, \quad (3)$$

where \mathbf{n} is the inner normal to the surface of the capillary; the superscripts $+$, s , and $-$ refer, respectively, to particles that are reflected, emitted diffusively from, and incident upon the surface; n_j^s is the number density of particles emitted diffusively in the j -th state, m_0 is the mass of a particle, and k_B is Boltzmann's constant.

We now consider the case of low radiation intensity I , in which $\kappa(\mathbf{v}) \ll 1$. Then the states of the components of the gas mixture are slightly nonequilibrium, and the distribution functions f_n and f_m can be represented in the form

$$f_j(\tilde{\mathbf{r}}, \mathbf{v}) = f_{j0}[1 + h_j(\tilde{\mathbf{r}}, \mathbf{v})], \quad (4)$$

where

$$f_{j0} = n_{j0} \left(\frac{m_0}{2\pi k_B T} \right)^{3/2} \exp\left(-\frac{m_0 v^2}{2k_B T}\right), \quad j = m, n,$$

f_{j0} is the Maxwell-Boltzmann equilibrium distribution, n_{j0} is the equilibrium number density of particles in the j -th state, $h_j(\tilde{\mathbf{r}}, \mathbf{v})$ is the perturbation of the distribution of the j -th component, and $\tilde{\mathbf{r}}$ is the two-dimensional radius vector in a plane perpendicular to the z axis.

The intensity of the radiation is assumed to be uniform across the capillary. The saturation parameter $\kappa(\mathbf{v})$ does not depend on the radial coordinate $\tilde{\mathbf{r}}$. In an optically thin medium, the radiation intensity changes very little over the length of the capillary, and therefore the dependence of the perturbation functions h_j on the longitudinal coordinate z can be neglected.

Under these assumptions, the kinetic equations (1), linearized with respect to the perturbation functions h_j , can be put into the following dimensionless form using McCormack's second-order model collision integrals:¹¹

$$\begin{aligned} \mathbf{c}_\perp \frac{\partial h_j}{\partial \mathbf{r}} + R_j h_j + \beta_j R_j \Gamma_m h_m \\ = R_j \Gamma_m j \frac{1}{2} \kappa(\mathbf{v}) \left(\frac{n_{i0}}{n_{j0}} - 1 \right) + 2R_j c_z \left[u_j - (u_j - u_i) \varphi_{ji}^{(1)} \right] \\ + 4c_r c_z R_j \left[(1 - \varphi_{jj}^{(3)} + \varphi_{jj}^{(4)} - \varphi_{ji}^{(3)}) \pi_{jrz} + \varphi_{ji}^{(4)} \pi_{irz} \right], \end{aligned} \quad (5)$$

where

$$\mathbf{c} = \frac{\mathbf{v}}{\bar{v}}, \quad \bar{v} = \sqrt{\frac{2k_B T}{m_0}}, \quad c_\perp^2 = c_r^2 + c_\varphi^2, \quad \beta_m = 1, \quad \beta_n = -1,$$

$$\mathbf{r} = \frac{\tilde{\mathbf{r}}}{R_0}, \quad R_j = \frac{\gamma_j}{\bar{v}} R_0, \quad \gamma_j = \gamma_{jj} + \gamma_{ji}, \quad \Gamma_m j = \frac{\Gamma_m}{\gamma_j}, \quad (6)$$

$$\varphi_{ji}^{(n)} = \frac{\nu_{ji}^{(n)}}{\gamma_j}, \quad \varphi_{jj}^{(n)} = \frac{\nu_{jj}^{(n)}}{\gamma_j},$$

$$u_j = \frac{U_j}{\bar{v}} = \int c_z E h_j d\mathbf{c}, \quad \pi_{jrz} = \frac{P_{jrz}}{2P_j} = \int c_r c_z E h_j d\mathbf{c},$$

$$E = \pi^{-3/2} \exp(-c^2), \quad (i, j) = m, n, \quad i \neq j,$$

U_j , P_{jrz} , and P_j are the partial velocity, stress tensor, and pressure of the j -th component of the mixture; γ_{jj} and γ_{ji} are the effective intermolecular elastic collision rates for collisions of type $j-j$ and $j-i$, respectively; R_j is a tenuousness parameter, which is inversely proportional to the Knudsen number (Kn is the ratio of the particle mean-free path l to the capillary radius R_0); expressions for the frequencies $\nu_{ji}^{(n)}$ in terms of the Chapman-Cowling integrals, which depend on the form of the intermolecular interaction potential, are presented in Ref. 11; \mathbf{c}_\perp is the two-dimensional component of the dimensionless velocity vector \mathbf{c} in a plane perpendicular to the z axis; and, c_r and c_φ are components of the vector \mathbf{c}_\perp .

The boundary conditions for the perturbation functions h_j follow from (2) and (4):

$$h_j^+(\mathbf{r}_0, \mathbf{c}) = (1 - \varepsilon_j) h_j^-(\mathbf{r}_0, \mathbf{c}) + \varepsilon_j \frac{n_j^s - n_{j0}}{n_{j0}}, \quad (7)$$

$$\mathbf{r}_0 = \mathbf{R}_0/R_0, \quad |\mathbf{r}_0| = 1, \quad j = m, n.$$

The second term on the right-hand side of (7) does not depend on the molecular velocities, and consequently it does not contribute to the macroscopic velocity and stress tensor (6). It will therefore be dropped in the subsequent discussion.

It should be noted that the probability of stimulated transitions is small under low-intensity irradiation. Then the ratio n_m/n_n is also a small quantity, i.e., $\alpha_m = n_m/n_n \ll 1$.

Equations (5)–(7) make it possible to determine the functions $h_j(\mathbf{r}, \mathbf{c})$ uniquely. However, it is of practical interest to determine the resulting particle flux (light-induced drift) averaged over the transverse cross section of the capillary:

$$J = J_m + J_n = 2\bar{v} \int_0^1 (n_n u_n + n_m u_m) r dr. \quad (8)$$

For numerical calculations it is convenient to use the dimensionless quantity G , which is related to the flux J by

$$J = \frac{\dot{n} R_0 \Gamma_m}{2} \kappa G, \quad (9)$$

where

$$\kappa = \frac{1}{\sqrt{\pi}} \int_{-\infty}^{\infty} c_z \exp(-c_z^2) \kappa(\mathbf{v}) dc_z. \quad (10)$$

We now transform to a new coordinate system in velocity space: we replace the independent variables c_r and c_φ by the variables c_\perp and θ defined as follows:

$$c_\perp = \sqrt{c_r^2 + c_\varphi^2}, \quad \theta = \arctan(c_\varphi/c_r). \quad (11)$$

Since the longitudinal component c_z of the molecular velocity appears in Eq. (5) as a parameter, we introduce the following truncated perturbation functions:

$$\Phi_j(r, c_\perp, \theta) = \frac{\alpha_j}{\sqrt{\pi} \Gamma_{mj} R_j \kappa} \int_{-\infty}^{\infty} h_j(\mathbf{r}, \mathbf{c}) \exp(-c_z^2) c_z dc_z, \quad (12)$$

where $\alpha_n = 1$ and $\alpha_m = n_m/n_n$.

We also introduce, in accordance with (6) and (12), new functions for the macroscopic velocities and viscous stresses:

$$w_j(r) = \frac{\alpha_j \mu_j(r)}{\kappa \Gamma_{mj} R_j} = \frac{1}{\pi} \int_0^\infty \int_0^{2\pi} \Phi_j(r, c_\perp, \theta) \times \exp(-c_\perp^2) c_\perp dc_\perp d\theta, \quad (13)$$

$$t_j(r) = \frac{\alpha_j \pi j r z(r)}{\kappa \Gamma_{mj} R_j} = \frac{1}{\pi} \int_0^\infty \int_0^{2\pi} \Phi_j(r, c_\perp, \theta) \times \exp(-c_\perp^2) c_\perp^2 \cos \theta dc_\perp d\theta. \quad (14)$$

Neglecting terms of order α_m and taking (11)–(14) into consideration, we obtain from (5) the following kinetic equations for the truncated perturbation functions Φ_m and Φ_n :

$$\begin{aligned} c_\perp \cos \theta \frac{\partial \Phi_n}{\partial r} - c_\perp \frac{\sin \theta}{r} \frac{\partial \Phi_n}{\partial \theta} + R_n \Phi_n \\ = -\frac{1}{2} + \Gamma_{mn} R_n \Phi_m + R_n w_n + R_m (\varphi_{mn}^{(1)} w_m \\ + 2c_\perp \varphi_{mn}^{(4)} t_m \cos \theta) + 2R_n c_\perp (1 - \varphi_{nn}^{(3)} + \varphi_{nn}^{(4)}) t_n \cos \theta, \end{aligned} \quad (15)$$

$$\begin{aligned} c_\perp \cos \theta \frac{\partial \Phi_m}{\partial r} - c_\perp \frac{\sin \theta}{r} \frac{\partial \Phi_m}{\partial \theta} + R_m \Phi_m \\ = \frac{1}{2} - \Gamma_{mm} R_m \Phi_m + R_m (1 - \varphi_{mn}^{(1)}) w_m \\ + 2R_m c_\perp (1 - \varphi_{mn}^{(3)}) t_m \cos \theta. \end{aligned} \quad (16)$$

On the basis of (12), the boundary conditions (7) assume the form

$$\Phi_j^+(\mathbf{r}_0, c_\perp, \theta) = (1 - \varepsilon_j) \Phi_j^-(\mathbf{r}_0, c_\perp, \theta), \quad j = m, n. \quad (17)$$

It is well known that for gas motion in a capillary, the accommodation coefficients ε_j are close to unity,¹² while the relative difference between the effective diameters of excited (σ_m) and unexcited (σ_n) particles is small¹³:

$$1 - \varepsilon_j \ll 1, \quad |\Delta \sigma|/\sigma_n \ll 1, \quad \Delta \sigma = \sigma_m - \sigma_n, \quad j = m, n. \quad (18)$$

We choose the effective collision rate by analogy with the Bhatnagar–Gross–Krook model in the form $\gamma_n = p/\eta$, where η is the dynamic viscosity coefficient and p is the pressure. We model the gas particles as hard elastic spheres with effective diameters σ_m and σ_n for the excited and unexcited particles, respectively. Then the rarefaction parameter R_n is related to the Knudsen number by¹²

$$R \equiv R_n = \frac{\sqrt{\pi}}{2} \text{Kn}^{-1}, \quad \text{Kn} = \frac{l}{R_0}. \quad (19)$$

By virtue of the inequalities (18), we have

$$S = \frac{R_m}{R_n} = \frac{\gamma_{mn}}{\gamma_{nn}} = \frac{\sigma_{mn}^2}{\sigma_n^2} \approx 1 + \frac{\Delta \sigma}{\sigma_n}, \quad \sigma_{mn} = \frac{\sigma_m + \sigma_n}{2}. \quad (20)$$

As a result, we obtain from Eqs. (15) and (16) for the hard-sphere molecular model

$$\begin{aligned} c_\perp \cos \theta \frac{\partial \Phi_n}{\partial r} - c_\perp \frac{\sin \theta}{r} \frac{\partial \Phi_n}{\partial \theta} + R \Phi_n \\ = -\frac{1}{2} + \Gamma_{mn} R \Phi_m + R \left(w_n + \frac{5}{6} S w_m \right) + \frac{2}{3} R c_\perp S t_m \cos \theta, \end{aligned} \quad (21)$$

$$\begin{aligned} c_\perp \cos \theta \frac{\partial \Phi_m}{\partial r} - c_\perp \frac{\sin \theta}{r} \frac{\partial \Phi_m}{\partial \theta} + R \Phi_m S \\ = \frac{1}{2} - \Gamma_{mn} R \Phi_m + \frac{1}{6} S w_m R - \frac{2}{3} R c_\perp S t_m \cos \theta. \end{aligned} \quad (22)$$

Here the fact that $t_n = -t_m$ as a result of momentum conservation has been taken into account.⁷

Linearizing with respect to the small parameters (18) makes it possible to separate the surface and collisions mechanisms of light-induced drift. Then

$$w_j(r) = w_{1j}(r)\Delta\varepsilon + w_{2j}(r)\frac{\Delta\sigma}{\sigma_n}, \quad \Delta\varepsilon = \varepsilon_n - \varepsilon_m, \quad j = n, m, \quad (23)$$

$$G(R, \Gamma_{mn}) = G_1(R, \Gamma_{mn})\Delta\varepsilon + G_2(R, \Gamma_{mn})\frac{\Delta\sigma}{\sigma_n}. \quad (24)$$

The kinetic coefficients G_1 and G_2 , which characterize the respective contributions of the surface and collisional mechanisms to light-induced drift, depend only on the rarefaction parameter R and the Γ_{mn} —the ratios of the radiative decay rate Γ_m of the excited level to the intermolecular collision rate γ_n . In the approximation (18), the kinetic equations do not depend on ε_j and $\Delta\sigma/\sigma_n$.

Substituting (24) into Eq. (9) gives the following expression for the light-induced drift flux:

$$J = \frac{nR_0\Gamma_m\kappa}{2} \left(G_1\Delta\varepsilon + G_2\frac{\Delta\sigma}{\sigma_n} \right). \quad (25)$$

3. SOLUTION OF THE KINETIC EQUATIONS

To solve Eqs. (21) and (22) with the boundary conditions (17), we employ the numerical method of discrete ordinates, which is based on replacing the continuous phase space by a discrete phase space. In so doing it is assumed that the gas molecules cannot move with arbitrary velocities, but only with velocities from a fixed set, which comprises $c_{\perp i}$ ($i = 1, \dots, N_c$) and θ_q ($q = 1, \dots, N_t$). This set forms the nodes of a computational mesh in molecular velocity space. We also introduce a discrete configuration space with nodes r_k ($k = 1, \dots, N_r$).

Then the finite-difference scheme for Eqs. (21) and (22) takes the form

$$c_{\perp i} \cos \theta_q \frac{\Phi_n^{kiq} - \Phi_n^{k-1,i,q}}{\Delta r} - c_{\perp i} \frac{\sin \theta_q}{r_k} \frac{\Phi_n^{kiq} - \Phi_n^{ki,q-1}}{\Delta \theta} + R\Phi_n^{kiq} = -\frac{1}{2} + R\Gamma_{mn}\Phi_m^{kiq} + R \left(w_n^k + \frac{5}{6} w_m^k S + \frac{2}{3} c_{\perp i} S t_m^k \cos \theta_q \right), \quad (26)$$

$$c_{\perp i} \cos \theta_q \frac{\Phi_m^{kiq} - \Phi_m^{k-1,i,q}}{\Delta r} - c_{\perp i} \frac{\sin \theta_q}{r_k} \frac{\Phi_m^{kiq} - \Phi_m^{ki,q-1}}{\Delta \theta} + R\Phi_m^{kiq} S = \frac{1}{2} - R\Gamma_{mn}\Phi_m^{kiq} + R \left(\frac{1}{6} w_m^k S - \frac{2}{3} c_{\perp i} S t_m^k \cos \theta_q \right), \quad (27)$$

$$k = 1, \dots, N_r, \quad i = 1, \dots, N_c, \quad q = 1, \dots, N_t.$$

Here Φ_n^{kiq} and Φ_m^{kiq} are the values of the truncated perturbation functions (12) at the nodes, i.e.,

$$\Phi_j^{kiq} \equiv \Phi_j(r_k, c_{\perp i}, \theta_q), \quad j = n, m.$$

The points r_k are distributed uniformly over the closed interval $[0, 1]$ such that $r_0 = 1$, $r_k = r_{k-1} - \Delta r$, and $\Delta r = 1/N_r$; the nodes $\theta_q = \theta_{q-1} + \Delta \theta$ lie in the closed interval $[0, 2\pi]$, with $\Delta \theta = 2\pi/N_t$; the points $c_{\perp i}$ are Gaussian nodes, which determine the values of the dimensionless velocity c_{\perp} of the molecules in the interval $(0, \infty)$. The dimensionless macroscopic velocities $w_j^k \equiv w_j(r_k)$ and the tangential stresses $t_j^k \equiv t_j(r_k)$ for the excited ($j = m$) and unexcited ($j = n$) particles at any point r_k of the transverse cross section of a capillary are calculated using (13) and (14) with the following quadrature formulas:

$$w_j^k = \frac{1}{\pi} \sum_i^{N_c} \sum_q^{N_t} \Phi_j^{kiq} W_i^c \Delta \theta, \quad j = n, m, \quad (28)$$

$$t_m^k = \frac{1}{\pi} \sum_i^{N_c} \sum_q^{N_t} \Phi_m^{kiq} W_i^t \Delta \theta \cos \theta_q, \quad (29)$$

where W_i^c and W_i^t are the Gaussian weights for the velocities and stresses.

The boundary conditions (17) become

$$\Phi_j^+(c_{\perp i}, \theta_q^+, r_0 = 1) = (1 - \varepsilon_j) \Phi_j^-(c_{\perp i}, \theta_q^-, r_0 = 1), \quad (30)$$

$$k = 0, \quad i = 1, \dots, N_c, \quad q = 0, \dots, N_t, \quad j = n, m,$$

the points θ_q^+ , which determine the directions of the velocities of the molecules reflected from the surface of the capillary, lie in the interval $(\pi/2, 3\pi/2)$, and the points θ_q^- for the molecules incident on the surface lie in the interval $(-\pi/2, +\pi/2)$.

Equations (26)–(30) were solved by iterative refinement. Using the zeroth approximation ($p = 0$) for certain (generally arbitrary) profiles of the partial macroscopic velocities and the stress tensor, the values of Φ_j^{kiq} can be obtained by iteration to any higher approximation. The new values of the macroscopic quantities $w_j^{k(p)}$ and $t_m^{k(p)}$ are calculated from the formulas (28) and (29) at each iteration step ($p > 0$). The rate of convergence of the iteration process depends largely on the choice of the zeroth approximation. In the present work the equilibrium state of the gas, in which

$$w_j^{k(0)} = 0, \quad t_m^{k(0)} = 0,$$

was chosen as the zeroth approximation. The iterations were continued until the relative difference between the computed values of the macroscopic parameters in the p -th and $(p-1)$ -th approximations was less than a prescribed value $\varepsilon = 10^{-6}$.

A nonuniform mesh, consisting of $N_c = 11$ Gaussian nodes, was used for the variable c_{\perp} , and a uniform mesh with $N_t = 20$ nodes was used for the variable θ . The mesh in configuration space consisted of $N_r = 200$ nodes, distributed uniformly along the radius of the capillary. The computational error was at most 0.1% for any values of the rarefaction parameter R and rate parameter Γ_{mn} .

The computational results are displayed in Figs. 1–4. Some of the computed values of the kinetic coefficients $G_1(R, \Gamma_{mn})$ and $G_2(R, \Gamma_{mn})$ are presented in Tables I and II.

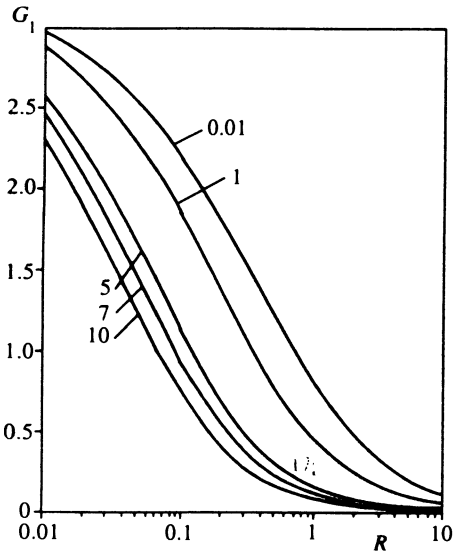


FIG. 1. Kinetic coefficient $G_1(R, \Gamma_{mn})$ or surface light-induced drift.

4. RESULTS AND COMPARISON WITH EXPERIMENT

The direction of the surface component of light-induced drift is determined by the signs of the difference $\Delta\varepsilon = \varepsilon_n - \varepsilon_m$ between the accommodation coefficients of the unexcited and excited particles, and the frequency offset $\Omega = \omega - \omega_{mn}$ of the radiation from the center of the absorption line. If $\Delta\varepsilon > 0$, the surface component of drift is oriented in the direction of the radiation for $\Omega > 0$, and opposite the radiation for $\Omega < 0$.

Figure 1 displays the kinetic coefficient G_1 , which characterizes the surface light-induced drift velocity as a function of the rarefaction parameter R for various values of the frequency parameter Γ_{mn} . Clearly G_1 decreases monotonically as the Knudsen regime passes into the hydrodynamic regime. The decrease in surface drift velocity with increasing Γ_{mn}

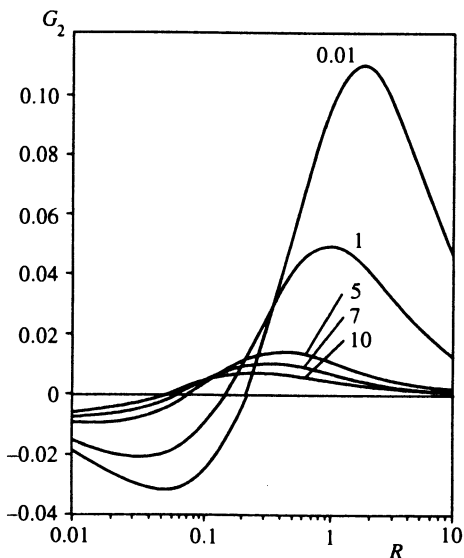


FIG. 2. Kinetic coefficient G_2 as a function of the rarefaction parameter R and the frequency parameter Γ_{mn} (curve labels).

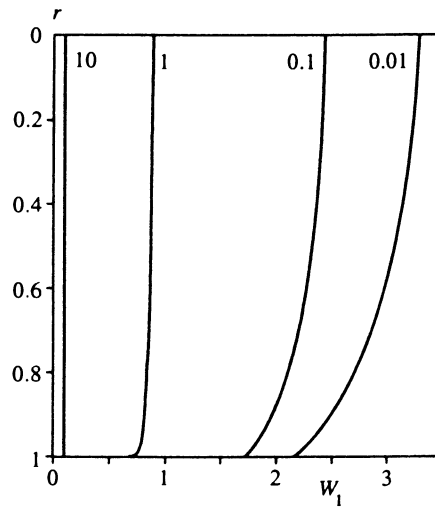


FIG. 3. Dimensionless velocity w_1 as a function of the radial coordinate r for $\Gamma_{mn} = 0.01$ and various values of R (curve labels).

and fixed R is explained by a decrease in the relative number of excited particles that collide with the capillary walls.

For fixed Γ_{mn} , the R -dependence of the kinetic coefficient G_2 , which characterizes the collisional light-induced drift, is nonmonotonic (Fig. 2). The curve $G_2(R)$ has a maximum and a minimum, and for some value $R^{(0)}(\Gamma_{mn})$ of the rarefaction parameter, the coefficient G_2 changes sign. This means that the direction of the collisional component of light-induced drift is determined not only by the sign of the frequency offset Ω from the center of the absorption line, but by the gas pressure in the capillary as well. A possible reason for this behavior of $G_2(R)$ is discussed in detail in Ref. 9 for $\Gamma_{mn} \ll 1$, where the inversion value $R^{(0)}$ of the rarefaction parameter R is fixed. In the general case, the collisional

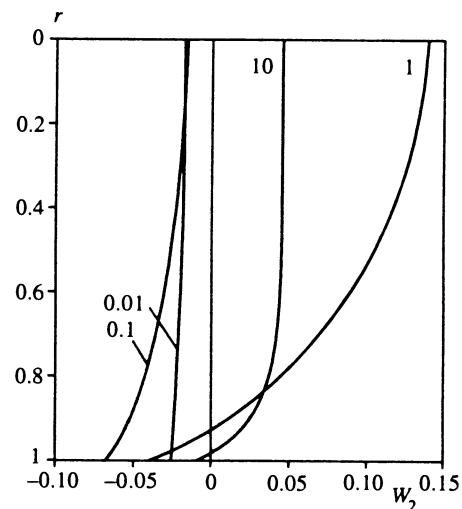


FIG. 4. Dimensionless velocity w_2 as a function of the radial coordinate r for $\Gamma_{mn} = 0.01$ and various values of R (curve labels).

TABLE I. Kinetic coefficient $G_1(R, \Gamma_{mn})$ for surface light-induced drift.

R	Γ_m				
	0.01	1	5	7	10
0.01	2.975	2.879	2.585	2.469	2.319
0.04	2.635	2.413	1.834	1.641	1.417
0.07	2.416	2.124	1.442	1.240	1.020
0.1	2.249	1.911	1.188	0.992	0.791
0.2	1.867	1.451	0.738	0.583	0.440
0.3	1.616	1.174	0.527	0.407	0.300
0.4	1.430	0.983	0.406	0.310	0.227
0.7	1.068	0.654	0.238	0.179	0.130
1.0	0.849	0.485	0.168	0.126	0.0912
2.0	0.494	0.254	0.0840	0.0629	0.0456
3.0	0.343	0.171	0.0560	0.0419	0.0304
5.0	0.210	0.103	0.0336	0.0251	0.0182
7.0	0.150	0.073	0.0240	0.0179	0.0130
10.0	0.105	0.0514	0.0167	0.0125	0.0091

light-induced drift reverses direction at $R^{(0)} \approx 0.05 - 0.25$, depending on the value of the frequency parameter Γ_{mn} (Fig. 2). Thus, the direction of collisional light-induced drift at fixed gas pressure in the capillary is also determined by the magnitude of the radiative decay constant Γ_m .

It can be seen from Fig. 2 that the greater the value of Γ_{mn} , i.e., the fewer the collisions an excited particle undergoes on average before being quenched, the smaller the value of the kinetic coefficient G_2 . In the limit $\Gamma_{mn} \rightarrow \infty$, there is enough time for all excited particles to decay to the ground state during the time taken to cover one mean free path length, and there is therefore no collisional light-induced drift.

Note that for $\Gamma_{mn} \leq 0.1$, the kinetic coefficients G_1 and G_2 do not depend on Γ_{mn} . In this range of values of Γ_{mn} , the results of Ref. 9 are valid.

Figures 3 and 4 display the dimensionless macroscopic velocities w_1 and w_2 as functions of the radial coordinate r . One can see (Fig. 3) that the surface component w_1 of the

velocity for $R \geq 1$ remains essentially constant across the capillary. This suggests that the viscosity of the gas does not greatly affect the surface light-induced drift.

Note that the surface drift velocity calculated in Ref. 4 has the typical parabolic profile of standard Poiseuille flow. The evolution of the profile of the collisional component w_2 of the velocity as the free-molecular regime passes into the hydrodynamic regime is interesting (Fig. 4). As long as the rarefaction parameter R is small, w_2 will be virtually independent of r . For $R > 0.10$, the structure of the light-induced drift flow becomes more complicated. A "core" of the flow, directed in one direction, forms near the axis of the capillary, while in the layer near the wall the gas moves in the opposite direction. The existence of a counterflow is related to the fact that the flux of the excited particles near the wall for intermediate values of R is higher than the flux of unexcited particles, and conversely near the axis of the capillary. In the almost free-molecular regime ($R \leq 0.1$), the velocity w_2 is directed opposite the wave vector \mathbf{k} , and w_2 is

TABLE II. Kinetic coefficient $G_2(R, \Gamma_{mn})$, 10^{-2} , for collisional light-induced drift.

R	Γ_{mn}				
	0.01	1	5	7	10
0.01	-1.916	-1.581	-0.946	-0.785	-0.619
0.03	-2.995	-2.135	-0.881	-0.620	-0.377
0.05	-3.206	-2.059	-0.558	-0.295	-0.079
0.07	-3.132	-1.787	-0.228	-0.003	0.154
0.1	-2.749	-1.251	0.196	0.336	0.393
0.2	-0.781	0.590	1.020	0.878	0.683
0.3	1.276	2.017	1.326	1.011	6.699
0.4	3.098	3.032	1.412	1.006	0.652
0.7	6.952	4.557	1.294	0.834	0.493
1.0	9.144	4.946	1.096	0.682	0.385
2.0	10.969	4.324	0.675	0.396	0.217
3.0	10.207	3.463	0.478	0.275	0.149
5.0	7.957	2.353	0.295	0.169	0.091
7.0	6.254	1.743	0.211	0.120	-
10.0	4.619	1.237	0.147	0.083	0.044

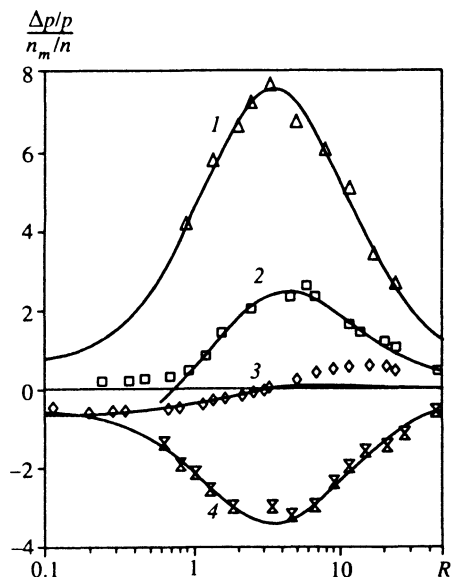


FIG. 5. Comparison of theory (solid lines) with experimental data for CH_3F molecules: 1) $P(24, 13)$; 2) $Q(12, 3)$; 3) $R(4, 3)$; 4) $R(31, 9)$.

greater near the wall than on the axis of the capillary (concave profile). In the hydrodynamic regime, for $R > 10$, the velocity w_2 is oriented in the same as the direction as the wave vector \mathbf{k} , and w_2 increases away from the wall.

Light-induced drift has been studied experimentally¹³ in CH_3F molecules. Resonant CO_2 laser radiation was directed along a quartz capillary with radius $R_0 \approx 0.75$ mm and length $L \approx 300$ mm. The mean gas pressure in the cell was varied over the range 0.7–280 Pa, which corresponds to rarefaction parameters $R \approx 0.1$ –47.

The results of the measurements are presented in Ref. 13 for the quantity⁹

$$\frac{\Delta p/p}{n_m/n} = \frac{L}{R_0} \varphi(\Omega) \left(\frac{1}{2} + R \right) \left(P_1 \Delta \varepsilon + P_2 \frac{\Delta \sigma}{\sigma_n} \right),$$

$$P_1 = \frac{G_1}{G_p}, \quad P_2 = \frac{G_2}{G_p}, \quad (31)$$

where $\varphi(\Omega)$ is an antisymmetric function of the detuning Ω (Ref. 14), and G_p is a kinetic coefficient that characterizes Poiseuille flow and depends on the parameters R and ε_n .¹²

TABLE III. Parameters $\Delta \varepsilon = \varepsilon_n - \varepsilon_m$ and $\Delta \sigma / \sigma_n = (\sigma_m - \sigma_n) / \sigma_n$ reconstructed from experiments on light-induced drift of CH_3F molecules in a quartz capillary.

Branch	$R(4, 3)$	$R(31, 9)$	$Q(12, 3)$	$P(24, 13)$
$\Delta \varepsilon, 10^{-3}$	-1.65	-(2.5-3)	7.3-8.1	-(2.1-3.3)
$\Delta \sigma / \sigma_n, 10^{-3}$	5.08	-(50-64)	-(103-112)	-(59.9-90.5)

In Fig. 5 the theoretical results are compared with the experiment of Ref. 13. The values chosen for the parameters $\Delta \varepsilon$ and $\Delta \sigma / \sigma_n$ are presented in Table III. The small discrepancy with the results of Ref. 9 results from our more accurate numerical calculation, and the uncertainty in the values is due to the experimental uncertainty in the homogeneous half-width Γ of the absorption line, and thus the function $\varphi(\Omega)$.¹⁴ The theoretical curves corresponding to the Eq. (31) satisfactorily describe the experimental data at all pressures.

Financial support for this work was provided by the International Science Foundation (grant No. RG4000).

¹A. V. Ghiner, M. I. Stockman, and M. A. Vaksman, *Phys. Lett A* **96**, 79 (1983).

²V. V. Levdanskiĭ, *Zh. Tekh. Fiz.* **53**, 810 (1983) [*Sov. Phys. Tech. Phys.* **28**, 518 (1983)].

³A. M. Dykhne and A. N. Starostin, *Zh. Éksp. Teor. Fiz.* **79**, 1211 (1980) [*Sov. Phys. JETP* **52**, 612 (1980)].

⁴M. A. Vaksman and A. V. Gaĭner, *Zh. Éksp. Teor. Fiz.* **89**, 41 (1985) [*Sov. Phys. JETP* **62**, 23 (1985)].

⁵A. E. Bazelyan and M. N. Kogan, *Dokl. Akad. Nauk SSSR* **308**, 75 (1989) [*Sov. Phys. Dokl.* **34**, 770 (1989)].

⁶I. V. Chernyaninov and V. G. Chernyak, *Inzh.-Fiz. Zh.* **60**, 1015 (1991).

⁷V. G. Chernyak, I. V. Chernyaninov, E. A. Vilisova, and E. A. Subbotin, *Prikl. Mekh. Tekh. Fiz.*, No. 5, 3 (1994).

⁸V. M. Zhdanov, A. A. Krylov, and V. I. Roldugin, *Zh. Éksp. Teor. Fiz.* **105**, 94 (1994) [*JETP* **78**, 49 (1994)].

⁹V. G. Chernyak, E. A. Vintovkina, and I. V. Chernyaninov, *Zh. Éksp. Teor. Fiz.* **103**, 1571 (1993) [*JETP* **76**, 768 (1993)].

¹⁰S. G. Rautian, G. I. Smirnov, and A. M. Shalagin, *Nonlinear Resonances in Atomic and Molecular Spectra* [in Russian], Nauka, Novosibirsk (1979).

¹¹F. J. McCormack, *Phys. Fluids* **16**, 2095 (1973).

¹²V. G. Chernyak, B. T. Porodnov, and P. E. Suetin, *Zh. Tekh. Fiz.* **43**, 2420 (1973) [*Sov. Phys. Tech. Phys.* **18**, 1526 (1973)].

¹³R. W. M. Hoogeveen, G. J. van der Meer, and L. J. F. Hermans, *Phys. Rev. A* **42**, 6471 (1990).

¹⁴V. R. Mironenko and A. M. Shalagin, *Izv. Akad. Nauk SSSR, Ser. Fiz.* **45**, 995 (1981).

Translated by M. E. Alferieff